THE JOURNAL OF PHYSICAL CHEMISTRY Letters

Letter

pubs.acs.org/JPCL

Understanding Adsorption-Induced Effects on Platinum Nanoparticles: An Energy-Decomposition Analysis

Federico Calle-Vallejo, Philippe Sautet, and David Loffreda*

Université de Lyon, CNRS, École Normale Supérieure de Lyon, Laboratoire de Chimie, 46 Allée d'Italie, 69364 Lyon, Cedex 07, France

Supporting Information

ABSTRACT: Platinum nanoparticle catalysts are used in a myriad of gas-phase, liquid-phase, and electrochemical reactions. Although a high catalytic activity is paramount, stability must also be guaranteed, especially when the nanoparticles are in contact with strongly bound adsorbates. Therefore, it is crucial to be able to accurately calculate adsorption-energy trends on Pt nanoparticles of multiple sizes and morphologies using ab initio methods at affordable computational expenses. Here, through an energy-decomposition analysis in which adsorption processes are regarded as the interplay between pure binding and various compensating core−shell deformations, we show that pure binding is responsible for the overall linear adsorption trends. Conversely, the energetic cost of the deformations is a site-independent, adsorbate-dependent constant value. These two observations and the description of the trends by means of generalized coordination numbers help to significantly reduce the computational expense of simulating large nanoparticles.

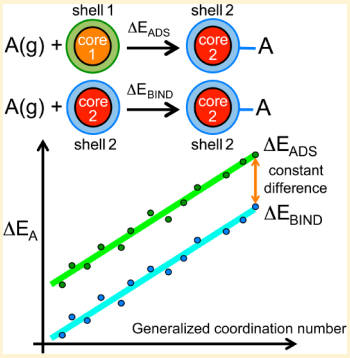

SECTION: Molecular Structure, Quantum Chemistry, and General Theory

Platinum and its alloys are active electrocatalysts for processes such as the oxygen reduction reaction,[1,2] hydrogen evolution reaction,[3] dimethyl ether oxidation,[4] nitrate and nitrite reduction,[5,6] among others. Whereas surface science studies are normally made on well-defined extended surfaces,[7] technological applications make use of multifaceted nanoparticles.[1,8] The presence of strain and finite-size effects can hinder the straightforward application of the conclusions drawn from extended surfaces to the design of nanoparticle catalysts.[9] Therefore, robust tools are required to describe the trends in catalytic activity of nanoparticles in simple terms and provide precise design principles.[10−13] Computationally speaking, fast descriptions of adsorption energies are needed to capture trends and provide explicit relationships between geometric structure and adsorption properties. In this context, generalized coordination numbers ($\overline{CN}$) have recently offered more accurate descriptions of trends in adsorption energies than conventional electronic-structure descriptors such as d-band centers, without resorting to knowledge of the density of states of the material,[14] thereby lowering the usual computational expenses.

Energy-decomposition analyses (EDAs) have been used for the past 30 years for quantifying different contributions to chemical bonding of molecular systems.[15,16] More recently, EDAs have been used in heterogeneous catalysis for the deconvolution of multiple effects influencing barrier heights of elementary reactions on flat and stepped surfaces of pure metals and alloys.[17−19] They have also been applied to the adsorption of large molecules, where the deformation energetics of the adsorbates strongly influence adsorption energies.[20−22] Here we show that beyond mere energetic differences, EDAs can also describe the trends in adsorption energies of O, O_2, OH, OOH, H_2O, and H_2O_2, that is, the ORR intermediates, on all sites on Pt nanoparticles by means of generalized coordination numbers.

To exemplify our approach, we have chosen the Pt_{201} nanoparticle (Figure 1), a truncated octahedron with a diameter of ∼1.7 nm, with alternating (111) and (100) terraces (denoted as 111T and 100T). Additional sites have been created by the deposition of one or two platinum adatoms in several positions. The generalized coordination numbers of all top, bridge, and hollow sites on Pt_{201} appear in Figure 1. These are calculated as a weighted average of the nearest neighbors of the active site, and the weights correspond to the usual coordination numbers of those neighbors, which allows for finite-size effects to be taken into account.[14] Further details of Pt_{201} and $\overline{CN}$ appear in the Supporting Information (SI).

The DFT adsorption energies are given as

$$\Delta E_{ADS} = E_{A@NP_2} - E_{NP_1} - E_{A(g)} \quad (1)$$

where 1 and 2 represent the conditions before and upon adsorption. Thus, NP_1 is the relaxed clean nanoparticle (Figure 2), $A@NP_2$ is the relaxed particle with species A adsorbed on it, and A is O, O_2, OH, OOH, H_2O, or H_2O_2. We divide Pt_{201} in a one-layer outer-shell and the complementary inner core (see Figure 2), and ΔE_{ADS} is decomposed into the following contributions

Received: June 20, 2014
Accepted: August 19, 2014
Published: August 19, 2014

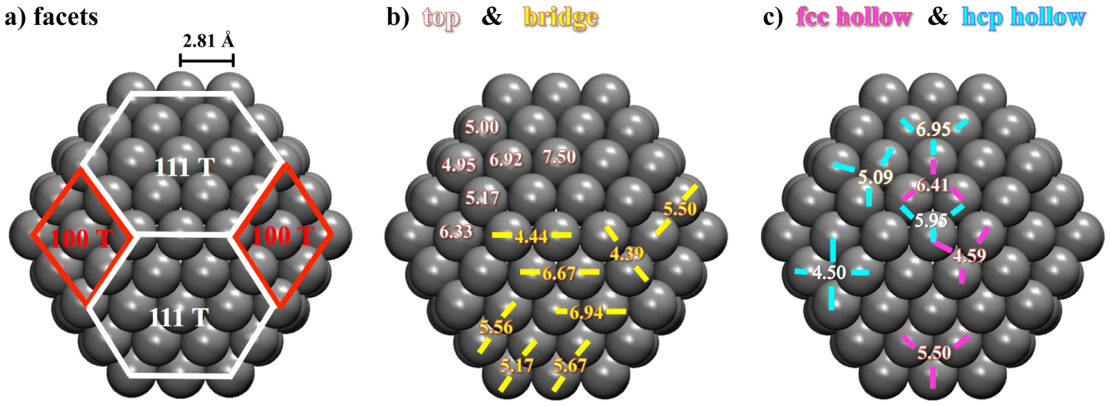

Figure 1. Perpendicular view to a (111) edge of Pt_{201}. (a) White and red lines delimitate (111) and (100) terraces. (b) $\overline{CN}$ for all inequivalent top (white) and bridge (yellow) sites. (c) $\overline{CN}$ for all inequivalent fcc (magenta) and hcp (blue) hollow sites. The lines in panels b and c indicate the surface atoms that form the sites.

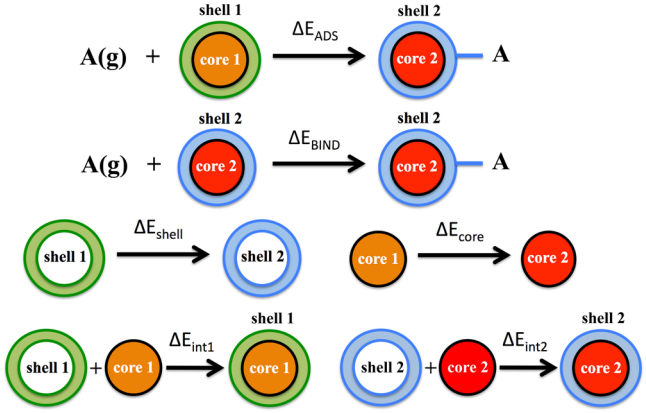

Figure 2. Schematics of the energy-decomposition analysis (EDA). Optimal geometries before adsorption are labeled "1" (orange/green for core/shell), whereas relaxed structures upon adsorption are labeled "2" (red/blue for core/shell).

$$\Delta E_{ADS} = \Delta E_{BIND} + \Delta E_{shell} + \Delta E_{core} + \Delta\Delta E_{int} \quad (2)$$

ΔE_{BIND} is the binding energy between species A and the isolated nanoparticle in the geometry of the relaxed adsorbed system (core 2 and shell 2, see Figure 2), and ΔE_{core} and ΔE_{shell} are the deformation energies of core and outer shell upon adsorption. The last term is the difference between the core−shell interaction terms upon and before adsorption: $\Delta\Delta E_{int} = \Delta E_{int2} - \Delta E_{int1}$. The interaction term is the energy gain resulting from the coupling of core and shell: $\Delta E_{int,i} = E_{NP,i} - E_{core,i} - E_{shell,i}$, where $i = 1, 2$. The equations in the EDA are schematized in Figure 2 and given in the SI.

The first point in this analysis is the comparison of binding and adsorption energies among the sites in Figure 1. Figure 3 summarizes the trends for all adsorbates in this study and shows that both energies follow similar linear relations with respect to $\overline{CN}$, with nearly identical slopes and only differences in the offsets. (See Table 1.) The only exception is *O, the trends of which will be discussed later. Note that if the differences are essentially constant, then

$$\Delta E_{ADS} - \Delta E_{BIND} = E_{NP_2} - E_{NP_1} \approx \kappa \quad (3)$$

where κ is an approximately constant value that depends on the adsorbate (see Table 1 and Figure S1 in the SI) but not on the adsorption site. Because E_{NP_1} is a common reference for all adsorption energies, E_{NP_2} must as well be nearly constant, implying that a given adsorbate deforms the particle with the same energy cost on all sites. On the basis of OH atop adsorption energies, Figure 3c,d shows that the constant difference holds for a wide range of particle sizes and various extended surfaces can also be included. The lower bound for this constant relation can be set at a particle size of ∼0.75 nm. This corresponds to Pt_{38}, the (111) terrace of which is the only outlier in Figure 3 (whereas its edges behave normally). To our knowledge, such a universality of the deformation energy upon adsorption had not been previously shown and justifies that densities of states be calculated on clean surfaces before adsorption and not including adsorbate-induced deformations.[14,23] The fact that deformation costs be roughly constant for dissimilar nanoparticle sites and sizes is important because it can save considerable computational expenses. For instance, entire nanoparticles can be frozen in the clean relaxed geometry, the adsorbates are relaxed, and the offset is added externally, which avoids the relaxation of hundreds of metal atoms. This is because $\overline{CN}$ captures finite-size effects,[14] and thus only one fully optimized calculation is required to determine the complete adsorption-energy trend with respect to it once the slope and the offset of the binding energy for the corresponding adsorbate are known.

The last part of our analysis shows that the energy shifts between adsorption and binding lines, although independent of site coordination, arise from complex energetic compensations within the nanoparticle, as illustrated in Figure 4.

Although the trends in this Figure are more complicated than those in Figure 3, several important observations can be made: (1) Core and shell deformation costs are mostly positive for all adsorbates and sites but differ by a factor of ∼4 (taken as the ratio of the maxima). (2) Core−shell interaction energies follow opposite trends compared with core and shell deformation costs. (3) Thus, the shapes of the three curves, that is, core and shell deformation and core−shell interactions, are such that their addition generates nearly flat lines for most adsorbates (see Figure S1 in the SI), which justifies the constant differences between binding and adsorption energies in Figure 3. (4) Weakly bound species, namely, $*H_2O$ and $*H_2O_2$, have nearly flat and small core−shell contributions, in line with their overall weak adsorption energies. (5) The extrema of the curves are around 2.7, 4.4, and 5.5, corresponding to adatoms on (100) terraces, (100) edges,

dx.doi.org/10.1021/jz501263e | J. Phys. Chem. Lett. 2014, 5, 3120−3124

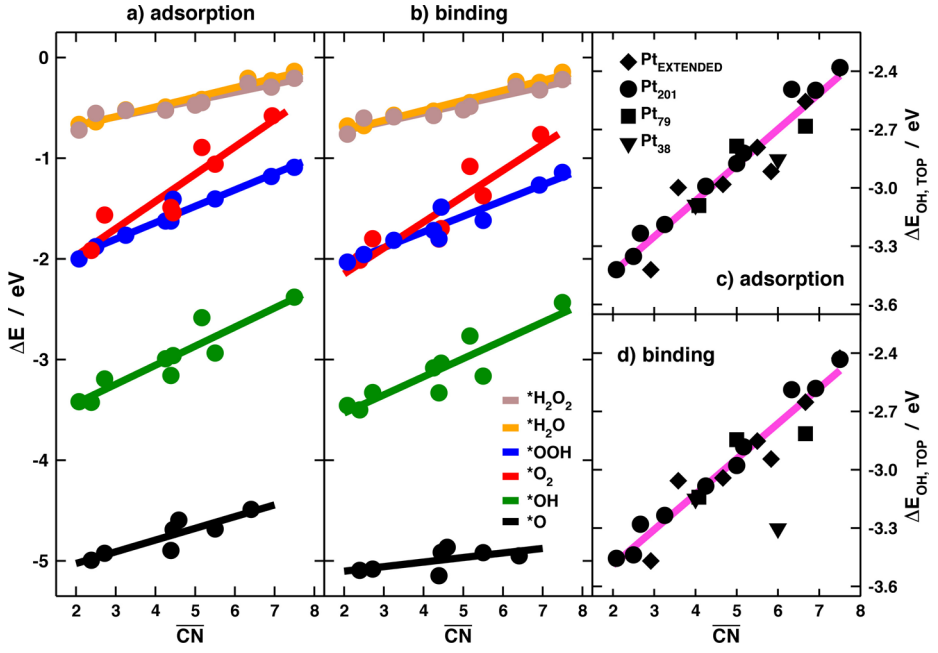

Figure 3. Trends in (a) adsorption energies (taken from ref 14) and (b) binding energies of various species on Pt_{201} as a function of $\overline{CN}$. Trends in (c) adsorption energies (taken from ref 14) and (d) binding energies of OH atop nanoparticles of several sizes and extended surfaces as a function of $\overline{CN}$. Additional data and parameters of the linear fits are given in Tables S2 and S3 in the SI.

Table 1. Adsorbate-Dependent Shifts between Adsorption and Binding Energies[a]

adsorbate	$\Delta E_{ADS} - \Delta E_{BIND} = \kappa$/eV	MAE/eV
H_2O	0.03	0.01
H_2O_2	0.04	0.01
OOH	0.10	0.06
OH (top)	0.07	0.03
OH	0.12	0.07
O_2	0.21	0.08
O	$0.074\overline{CN} - 0.078$	0.03

[a]Mean absolute errors are calculated as the difference between k and the actual differences from Figure 3.

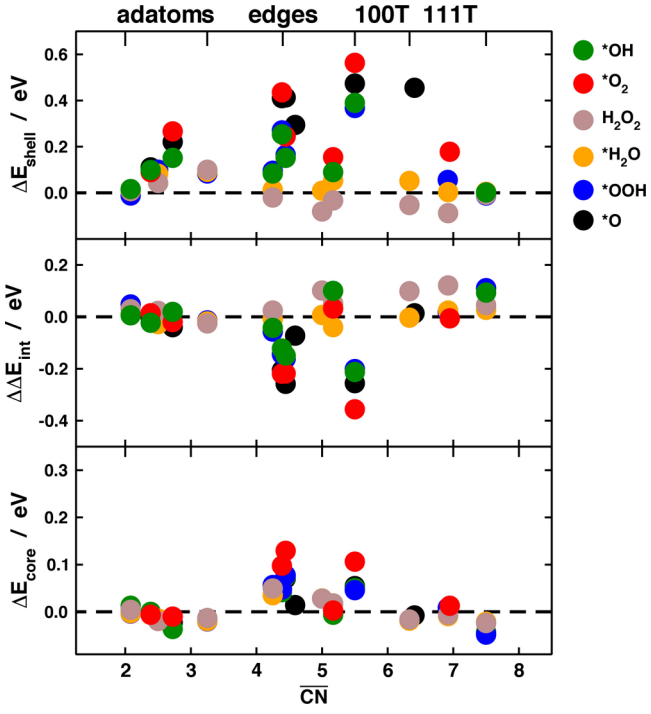

Figure 4. Evolution of the nanoparticle contributions to the adsorption energy as a function of $\overline{CN}$. Top: Energetic costs of adsorbate-induced deformations upon adsorption on the outer shell. Middle: Core/shell interaction energy. Bottom: Deformation energy costs on the core. The labels on the upper x axis illustrate the nanoparticle sites spanned by $\overline{CN}$.

and (100) terraces, respectively. This is useful to anticipate the structural behavior of the nanoparticle at high adsorbate coverages: the shell deformation will still be undergone because it is adsorbate-induced. Nevertheless, the compensating core−shell interactions might not be able to counteract the adsorbate-induced deformations, hence leading to surface reconstruction. Consequently, at high coverages, (100)-related geometries will presumably trigger the particle degradation.

Apart from *O, all adsorbates in this study are singly or doubly coordinated to the surface sites on Pt_{201}. However, *O binds to three-fold sites on (111) facets and to two-fold sites in all other facets and defects on Pt_{201}. The values for *OH and *OH(top) in Table 1 suggest that as more bonds are made to the surface, larger deformation costs are observed. Therefore, we attribute the unusual behavior of *O to its three-fold coordination to (111) sites. The fact that the differences between binding and adsorption follow a linear trend with respect to $\overline{CN}$ still allows for systematic corrections to be made. Future studies on N- and C-containing adsorbates will shed light on this respect.

In summary, we have extended EDAs to the many-site case of adsorption on nanoparticles using $\overline{CN}$ as a leading parameter. DFT calculations show that adsorbates, in order to optimize their interaction with the particle, induce a decrease in the stability of the outer shell. The instability created upon adsorption is partially counteracted by the change in the interaction between the outer shell and the rigid nanoparticle

dx.doi.org/10.1021/jz501263e | J. Phys. Chem. Lett. 2014, 5, 3120−3124

core. The net effect is a positive shift between binding and total adsorption energies that depends on the adsorbate but not on the adsorption site.

In view of the need for design principles for nanoparticle catalysts, we have provided here simple geometric structure versus adsorption/binding energy relations for oxygenates on Pt nanoparticles. With these, one can reduce the large computational expenses required to model adsorption processes on nanoparticles by freezing the metal atoms and adding external adsorbate-dependent corrections. Future studies should shed light on whether previously reported support effects[13] can also be systematized in the way shown here to extend our current understanding. Methodologically speaking, we have provided a simple way to extend EDAs from comparative analyses of a few data to systematic studies of trends arising from multifaceted and multisite materials.

COMPUTATIONAL METHODS

All DFT calculations were performed with VASP,[24] the PBE exchange-correlation functional,[25] and PAW potentials.[26] Geometry optimizations, during which all metal atoms and adsorbates were free to move in all directions, were made with the quasi-Newton scheme until the residual force on any atom was below 0.01 eV $Å^{-1}$. The nanoparticles were simulated in boxes of 26 Å × 26 Å × 26 Å, which ensured the convergence of adsorption energies within 0.05 eV. The plane-wave cutoff was 400 eV. The Methfessel−Paxton method was used to smear the Fermi level[27] with k_BT = 0.2 eV, and all energies were extrapolated to 0 K. The gas-phase references (O, O_2, OH, OOH, H_2O, and H_2O_2) were calculated in boxes of 15 Å × 15 Å × 15 Å, k_BT = 0.001 eV and spin polarization when appropriate. In all cases, the Brillouin zones were sampled with a gamma-point distribution. Isolated shells and cores were calculated through single-point calculations based on the converged geometries of the complete nanoparticle in its clean and upon-adsorption states. A discussion on the DFT-GGA errors associated with our results is given in the SI.

ASSOCIATED CONTENT

Supporting Information

Further information on generalized coordination numbers and Pt_{201}, the equations of the energy-decomposition analysis, additional details about Figure 3, and a brief comment on the DFT-GGA errors associated with the results. This material is available free of charge via the Internet at http://pubs.acs.org.

AUTHOR INFORMATION

Corresponding Author

*E-mail: david.loffreda@ens-lyon.fr.

Notes

The authors declare no competing financial interest.

ACKNOWLEDGMENTS

We acknowledge funding from the EU's FP7/2007-2013 program, call FCH-JU-2011-1 under grant agreement no. 303419. We thank IDRIS, CINES (project 609, GENCI/CT8), and PSMN for CPU time and assistance.

REFERENCES

(1) Katsounaros, I.; Cherevko, S.; Zeradjanin, A. R.; Mayrhofer, K. J. J. Oxygen Electrochemistry as a Cornerstone for Sustainable Energy Conversion. *Angew. Chem., Int. Ed.* **2014**, *53*, 102−121.

(2) Gasteiger, H. A.; Kocha, S. S.; Sompalli, B.; Wagner, F. T. Activity Benchmarks and Requirements for Pt, Pt-alloy, and Non-Pt Oxygen Reduction Catalysts for PEMFCs. *Appl. Catal., B* **2005**, *56*, 9−35.

(3) Greeley, J.; Jaramillo, T. F.; Bonde, J.; Chorkendorff, I.; Norskov, J. K. Computational High-Throughput Screening of Electrocatalytic Materials for Hydrogen Evolution. *Nat. Mater.* **2006**, *5*, 909−913.

(4) Li, H.; Calle-Vallejo, F.; Kolb, M. J.; Kwon, Y.; Li, Y.; Koper, M. T. M. Why (1 0 0) Terraces Break and Make Bonds: Oxidation of Dimethyl Ether on Platinum Single-Crystal Electrodes. *J. Am. Chem. Soc.* **2013**, *135*, 14329−14338.

(5) Yang, J.; Calle-Vallejo, F.; Duca, M.; Koper, M. T. M. Electrocatalytic Reduction of Nitrate on a Pt Electrode Modified by p-Block Metal Adatoms in Acid Solution. *ChemCatChem* **2013**, *5*, 1773−1783.

(6) Duca, M.; Rodriguez, P.; Yanson, A.; Koper, M. M. Selective Electrocatalysis on Platinum Nanoparticles with Preferential (100) Orientation Prepared by Cathodic Corrosion. *Top. Catal.* **2014**, *57*, 255−264.

(7) Climent, V.; Feliu, J. Thirty Years of Platinum Single Crystal Electrochemistry. *J. Solid State Electrochem.* **2011**, *15*, 1297−1315.

(8) Perez-Alonso, F. J.; Elkjær, C. F.; Shim, S. S.; Abrams, B. L.; Stephens, I. E. L.; Chorkendorff, I. Identical Locations Transmission Electron Microscopy Study of Pt/C Electrocatalyst Degradation During Oxygen Reduction Reaction. *J. Power Sources* **2011**, *196*, 6085−6091.

(9) Bandarenka, A. S.; Hansen, H. A.; Rossmeisl, J.; Stephens, I. E. L. Elucidating the Activity of Stepped Pt Single Crystals for Oxygen Reduction. *Phys. Chem. Chem. Phys.* **2014**, *16*, 13625−13629.

(10) Perez-Alonso, F. J.; McCarthy, D. N.; Nierhoff, A.; Hernandez-Fernandez, P.; Strebel, C.; Stephens, I. E. L.; Nielsen, J. H.; Chorkendorff, I. The Effect of Size on the Oxygen Electroreduction Activity of Mass-Selected Platinum Nanoparticles. *Angew. Chem., Int. Ed.* **2012**, *51*, 4641−4643.

(11) Tritsaris, G. A.; Greeley, J.; Rossmeisl, J.; Nørskov, J. K. Atomic-Scale Modeling of Particle Size Effects for the Oxygen Reduction Reaction on Pt. *Catal. Lett.* **2011**, *141*, 909−913.

(12) Solla-Gullon, J.; Vidal-Iglesias, F. J.; Lopez-Cudero, A.; Garnier, E.; Feliu, J. M.; Aldaz, A. Shape-Dependent Electrocatalysis: Methanol and Formic Acid Electrooxidation on Preferentially Oriented Pt Nanoparticles. *Phys. Chem. Chem. Phys.* **2008**, *10*, 3689−3698.

(13) Lim, D.-H.; Wilcox, J. Mechanisms of the Oxygen Reduction Reaction on Defective Graphene-Supported Pt Nanoparticles from First-Principles. *J. Phys. Chem. C* **2012**, *116*, 3653−3660.

(14) Calle-Vallejo, F.; Martínez, J. I.; García-Lastra, J. M.; Sautet, P.; Loffreda, D. Fast Prediction of Adsorption Properties for Platinum Nanocatalysts with Generalized Coordination Numbers. *Angew. Chem., Int. Ed.* **2014**, *53*, 8316−8319.

(15) Kitaura, K.; Morokuma, K. A New Energy Decomposition Scheme for Molecular Interactions within the Hartree-Fock Approximation. *Int. J. Quantum Chem.* **1976**, *10*, 325−340.

(16) Umeyama, H.; Morokuma, K. The Origin of Hydrogen Bonding. An Energy Decomposition Study. *J. Am. Chem. Soc.* **1977**, *99*, 1316−1332.

(17) Dupont, C.; Jugnet, Y.; Loffreda, D. Theoretical Evidence of PtSn Alloy Efficiency for CO Oxidation. *J. Am. Chem. Soc.* **2006**, *128*, 9129−9136.

(18) Loffreda, D.; Delbecq, F.; Simon, D.; Sautet, P. Breaking the NO Bond on Rh, Pd, and Pd3Mn Alloy (100) Surfaces: A Quantum Chemical Comparison of Reaction Paths. *J. Chem. Phys.* **2001**, *115*, 8101−8111.

(19) Hammer, B. Adsorption, Diffusion, and Dissociation of NO, N and O on Flat and Stepped Ru(0001). *Surf. Sci.* **2000**, *459*, 323−348.

(20) Haubrich, J.; Loffreda, D.; Delbecq, F.; Sautet, P.; Jugnet, Y.; Becker, C.; Wandelt, K. Adsorption and Vibrations of α,β-Unsaturated Aldehydes on Pt(111) and Pt−Sn Alloy (111) Surfaces. 3. Adsorption Energy vs Adsorption Strength. *J. Phys. Chem. C* **2009**, *114*, 1073−1084.

(21) Morin, C.; Simon, D.; Sautet, P. Density-Functional Study of the Adsorption and Vibration Spectra of Benzene Molecules on Pt(111). *J. Phys. Chem. B* **2003**, *107*, 2995−3002.
(22) Morin, C.; Simon, D.; Sautet, P. Chemisorption of Benzene on Pt(111), Pd(111), and Rh(111) Metal Surfaces: A Structural and Vibrational Comparison from First Principles. *J. Phys. Chem. B* **2004**, *108*, 5653−5665.
(23) Hammer, B.; Nørskov, J. K.; Bruce, C.; Gates, H. K. Theoretical Surface Science and Catalysis—Calculations and Concepts. *Adv. Catal.* **2000**, *45*, 71−129.
(24) Kresse, G.; Furthmüller, J. Efficient Iterative Schemes for Ab Initio Total-Energy Calculations Using a Plane-Wave Basis Set. *Phys. Rev. B* **1996**, *54*, 11169−11186.
(25) Perdew, J. P.; Burke, K.; Ernzerhof, M. Generalized Gradient Approximation Made Simple. *Phys. Rev. Lett.* **1997**, *78*, 1396−1396.
(26) Kresse, G.; Joubert, D. From Ultrasoft Pseudopotentials to the Projector Augmented-Wave Method. *Phys. Rev. B* **1999**, *59*, 1758−1775.
(27) Methfessel, M.; Paxton, A. T. High-precision Sampling for Brillouin-Zone Integration in Metals. *Phys. Rev. B* **1989**, *40*, 3616−3621.